Hindawi
Advances in Civil Engineering
Volume 2021, Article ID 1479196, 10 pages
https://doi.org/10.1155/2021/1479196

Research Article

A Study on Axial Compression Performance of Large Diameter-Thickness Ratio Concrete-Filled Gas Drainage Steel Pipe

Zi-Lu Liu, Zhan-Guo Ma, Ye Li, Peng Gong, Ke-Long Li, and Wang Liu

State Key Laboratory for Geomechanics and Deep Underground Engineering, School of Mechanics and Civil Engineering, China University of Mining and Technology, Xuzhou 221116, China

Correspondence should be addressed to Zhan-Guo Ma; zgma@cumt.edu.cn

Received 7 May 2021; Accepted 2 August 2021; Published 21 August 2021

Academic Editor: Fengqiang Gong

A large number of gas drainage pipes are obsoleted in the coal mine gas drainage system, and it causes serious waste. If concrete is poured into the discarded gas drainage pipes as components for underground roadway support, it is very significant for sustainable development of mine. Therefore, it is necessary to study the mechanical properties of the concrete-filled gas drainage steel pipe. Most frequently used gas drainage pipes are spiral welded steel pipe (SSP-I) and spiral external rib steel pipe (SSP-II). In this study, three different concrete-filled steel pipes are taken as the research object: SSP-I concrete-filled steel pipes, SSP-II concrete-filled steel pipes, and RSP concrete-filled ordinary round steel pipes. Through the axial compression test, the failure mode and relationship between stress-strain of concrete-filled steel pipes were obtained. Subsequently, the ultimate bearing capacity of three types of specimens was calculated based on the unified strength theory, limit equilibrium theory, and superposition theory. The test results show that both the SSP-I concrete-filled pipe columns and RSP concrete-filled pipe have good post-peak load-bearing capacity and ductility, and the second peak load reaches 70.38% and 81.92% of the ultimate load, respectively. The load-bearing capacity of SSP-II concrete-filled pipe columns is dropped sharply after bearing ultimate load, and the second peak load reaches only 36.47% of the ultimate load. The failure characteristics of concrete-filled gas drainage pipe columns show that the core concrete is compressed to powder and explain that the gas drainage pipe has fully exerted its restraint on the concrete. The FE method was used to simulate the compression test of three types of concrete-filled steel pipes, and the numerical simulation results show good agreement with the experimental results. Theoretical calculations show that the calculation of concrete-filled gas drainage pipe columns based on the superposition theory EC4-2004 is the closest to the measured value. Therefore, the EC4-2004 standard is recommended to calculate the ultimate bearing capacity of concrete-filled gas drainage pipe columns.

1. Introduction

Large amount of gas drainage pipes was equipped in the gas drainage system of coal mine. The most frequently used gas drainage pipes are spiral welded steel pipe (SSP-I) and spiral external rib steel pipe (SSP-II), and these gas drainage pipes have characters of large hoop stiffness and small wall thickness. Due to the long service period, abundant gas drainage pipes were discarded during the period of mining because their air tightness could not meet the safety requirements, and most of them cannot be repaired, and it causes serious waste, as shown in Figure 1.

The technology of gob-side entry retaining without coal pillar has been regarded as an important development direction of scientific mining due to its advantages of improving coal recovery rate, alleviating mining replacement contradiction, and optimizing working face ventilation mode [1–4], as shown in Figure 2. Roadside support body is the key of gob-side entry retaining technology, the traditional roadway side support body includes wooden pile, hydraulic column, gangue bag, concrete wall, and high water material filling wall. These traditional roadside support bodies have relative low support resistance but high labor intensity. Although high water and paste materials have

Figure 1: Large amount of abandoned gas drainage pipes in coal mines.

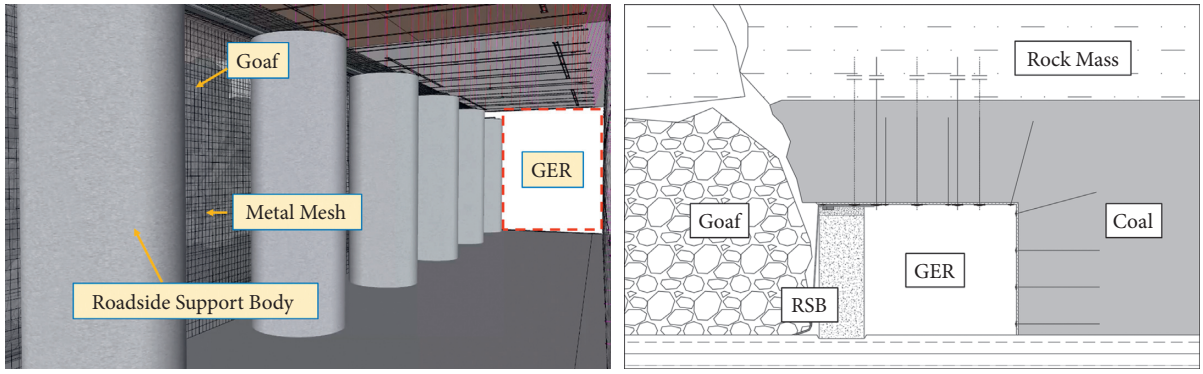

Figure 2: Layout of gob-side entry retaining.

perfect process flow, they have strict requirements for supporting equipment [5–8]. Concrete-filled steel pipe is a composite member made of concrete pouring in the steel pipe and concrete coordinated bearing the external load. The confinement effect of external steel pipe changes the concrete from two-way stress state to three-way stress state, which can improve the compressive properties of concrete. The internal concrete can improve the buckling of steel pipe and ensure the full play of material properties [9–11].

Concrete-filled steel pipe has been widely used in ground buildings due to its high strength and good ductility [9, 11–16]. In recent years, some scholars have begun to propose the introduction of concrete-filled steel pipe into coal mine roadway support. Huang et al. [17, 18] proposed a CSTC roadside support structure, which has achieved good application effect in gob-side entry retaining engineering of thick and hard roof roadway in A02 working face of Lu-Xi Mining Industry. Wang et al. [19] proposed a concrete-filled steel pipe composite roadway supporting structure, which has achieved good application effect in gob-side entry retaining of 2305S-2 # working face in Xinjulong Coal Mine. It can be seen that concrete-filled steel pipe as roadside support has good application prospect. If concrete can be poured into the discarded gas drainage pipe as the roadside support body of gob-side entry retaining, it will bring huge economic benefits to coal mining enterprises and solve the resulting environmental pollution problems.

In this paper, gas drainage pipes from Shanxi Lu'an Chemical Group Wang-Zhuang Coal Mine are taken, two types of gas drainage pipes (SSP-I, SSP-II) are used to make 6 concrete-filled steel pipe columns, 3 concrete-filled ordinary round steel pipe (RSP) columns with the same slenderness ratio are made, and experimental research on axial compression performance is carried out. Failure modes and stress-strain curve characteristics of the three specimens are compared and analyzed. Three types of specimens are calculated by the FE software, and the axial compression test of concrete-filled steel pipe was simulated and verified. Finally, the ultimate bearing capacity of the three types of specimens is calculated based on the unified strength theory, the limit equilibrium theory, and the superposition theory. It is of great significance to study the axial compression properties of concrete-filled gas drainage pipe columns for mine waste utilization and sustainable development.

2. Experiments

2.1. Sample Design. Three types of concrete-filled steel pipe short columns were designed: spiral welded steel pipe (SSP-I), spiral external rib steel pipe (SSP-II), and ordinary round steel pipe (RSP). The external diameter of the spiral welded steel pipe and the spiral external rib steel pipe is 430 mm, the wall thickness is 3 mm, and the height is 1300 mm. The ordinary round steel pipe has an outer diameter of 330 mm, the wall thickness is 5 mm, the height is 990 mm, and the concrete grade is C30, and the mix proportion of concrete is shown in Table 1.

The pipe is placed on a wooden backing board, and it is sealed with latex. The concrete is poured from the upper end

Table 1: Concrete mix ratio.

Cement (kg)	Sand (kg)	Stone (kg)	Accelerator (kg)	Early strength agent (kg)	Water (kg)
440	880	880	17.61	2.2	260

of the steel pipe, standard test cube blocks were reserved, and it was cured under the same conditions as the concrete-filled steel pipe columns. Design parameters for specimens are shown in Table 2. D is the external diameter of steel pipe; t is the thickness of steel pipe; α is steel content; $\alpha = A_s/A_c$, where A_s and A_c represent the sectional area of steel pipe and concrete, respectively; f_y and f_{cu} are yield strength and ultimate strength of steel pipe, respectively; E is the elastic modulus of steel pipe; ν is the Poisson ratio of steel pipes; ε_y is the yield strain of steel pipes; and ξ is the hoop constraint coefficient ($\alpha f_y/f_{cu}$).

2.2. Test Method. The test is carried out on a 600 t hydraulic press, the test loading system adopts load control, and the load of each class is $P_u/10$ (where P_u is the estimated ultimate load), last for 100 s. When the load reaches 0.9 P_u, it is converted to displacement control. When the load-displacement curve appears in a strengthening phase and the dial gauge reading is close to the maximum range, the load is terminated. The axial strain and circumferential strain of external steel pipe are automatically recorded and collected by static strain collector, the strain gauge is $H_{1\text{-}5}$ from the top to the bottom of the column, $H_{1\text{-}5}$-0 in the circumferential direction, and $H_{1\text{-}5}$-90 in the axial direction, the arrangement is shown in Figure 3(a), and the displacement data and load values are collected by dial indicator and computer, respectively, as shown in Figure 3(b).

3. Test Results

3.1. Sample Failure Form. At the beginning of loading, the appearance of the three types of specimens did not change. When the load increased to about 60% of the ultimate load, the inside of the two concrete-filled gas drainage steel pipe specimens began to make a colloidal cracking sound and the concrete-filled ordinary round steel pipe specimens did not variety. When the loading was continued to about 70%, the internal of the concrete-filled ordinary round steel pipe specimen began to make a sound of resin cracking. At this time, the middle and upper parts of the two kinds of concrete-filled gas drainage steel pipe column showed obvious wrinkles, accompanied by the sound of mutual extrusion and dislocation between concrete. When the load continued to increase to about 80% of the ultimate load, obvious bulging appeared in the middle of the concrete-filled ordinary round steel pipe specimens, and a large amount of surface rust dropped. The upper of two types of concrete-filled gas drainage steel pipes has deflection. When the load reached about 95% of the ultimate load, a bulging ring is formed on the upper surface of the ordinary round steel pipe, accompanied by the sound of concrete cracking. The two kinds of gas drainage steel pipe concrete specimens all appear to be oblique to the weld buckle within the full length, accompanied by the dull friction sound of the concrete and the steel pipe. The external ribs on the spiral external rib steel pipe surface are pulled off as shown in Figure 4. After the specimen reaches the ultimate load, the upper end of the ordinary round steel pipe is cracked and destroyed, accompanied by severe sound, and the cracking of internal concrete can be observed through the cracks in the steel pipe. Inclined triangle uplift appeared on the middle side of the two kinds of gas drainage pipes, and finally the specimen failed completely due to the excessive deformation of the steel pipe.

After the test, the specimen was lifted out of the test bench, and the failure mode of core concrete was observed. It was found that the concrete core in the upper part of the concrete-filled gas drainage steel pipes was pressed into powder. The buckling positions of concrete-filled spiral welded steel pipe column (SSP-I) specimens and ordinary concrete-filled steel pipe column specimens are mainly concentrated in the middle and upper parts, and the deformation of the lower part is small. The buckling positions of concrete-filled spiral external rib steel pipe column (SSP-II) specimens are uniformly distributed in the full-length range of the column. The external diameter changes of the upper loading end of the two types of steel pipes before and after failure were measured and compared. The external diameters of spiral welded pipe (SSP-I) and spiral external rib pipe (SSP-II) were 430 mm before loading and reached 479 mm and 492 mm, respectively, after loading, showing large transverse deformation.

3.2. Stress-Strain Relationship. The measured load and displacement of concrete-filled steel pipe columns are transformed into stress-strain curves, as shown in Figure 5.

$$\sigma = \frac{N}{A},$$
$$\varepsilon = \frac{\Delta l}{l}, \tag{1}$$

where N is the axial compressive force of the specimen; A is the total cross-sectional area of the specimen; Δl is the compressive displacement of the specimen in the stress process; and l is the height of the specimen.

The nominal stress-strain curves of three kinds of concrete-filled steel tubular columns can be divided into five stages: linear rise, slow growth, slow decline, secondary recovery, and rapid decline. From the perspective of the mechanical properties, this phenomenon reflects five stress stages: elastic stage, elastic-plastic stage, plastic stage, strengthening stage, and failure stage. In the elastic stage, the stress-strain curve of concrete-filled steel tubular short column increases linearly, and the elastic proportional limit load is about 70% of the ultimate load. When the specimen

Table 2: Design parameters for specimens.

No.	D (mm)	t (mm)	L/D	D/t	f_y (MPa)	f_{cu} (MPa)	E	α	ν	ε_y	ξ
SSP-I	430	3	3	141.6	235	30	189	0.028	0.29	1923	0.22
SSP-II	430	3	3	141.6	235	30	189	0.028	0.29	1923	0.22
RSP	330	5	3	66	235	30	161	0.059	0.27	1657	0.46

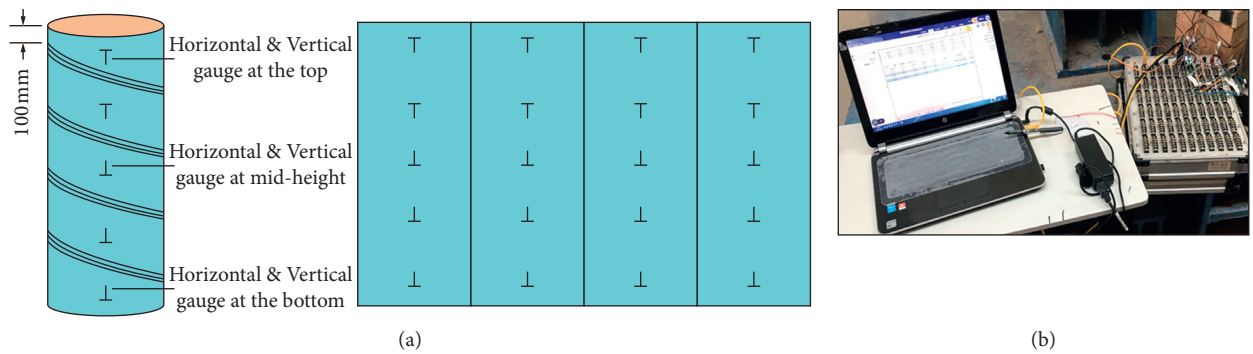

Figure 3: Schematic diagram of strain monitoring: (a) strain gauge layout; (b) static strain acquisition system.

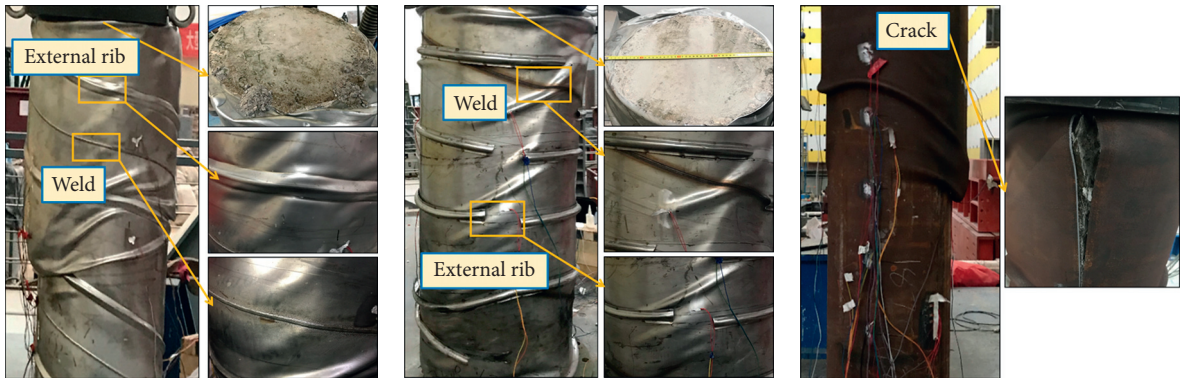

Figure 4: Failure modes of concrete-filled steel tubular columns with three cross sections: (a) SSP-I; (b) SSP-II; (c) RSP.

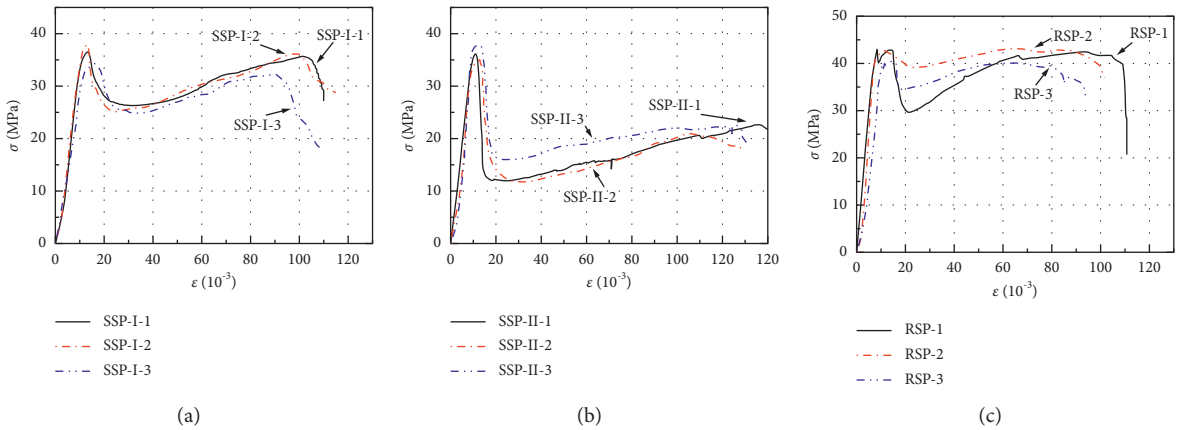

Figure 5: Stress-strain curve of concrete-filled steel tubular column: (a) SSP-I; (b) SSP-II; (c) RSP.

Table 3: Degradation range and recovery range of axial bearing capacity of specimens.

No.	SSP-I-1	SSP-I-2	SSP-I-3	SSP-II-1	SSP-II-2	SSP-II-3	RSP-1	RSP-2	RSP-3
First peak stress (MPa)	36.44	37.94	34.05	36.17	35.03	37.85	43.01	42.79	40.45
Valley stress (MPa)	26.23	25.16	24.81	11.92	11.77	16.01	29.65	39.17	34.49
Rising peak stress (MPa)	35.67	36.15	33.06	22.65	20.93	22.49	42.44	43.14	40.13
X (%)	71.95	66.33	72.88	33.56	33.60	42.27	68.93	91.53	85.26
ψ (%)	97.87	95.30	97.10	62.61	59.75	59.40	98.67	100.8	99.13

enters the elastic-plastic stage, plastic deformation begins to appear on the surface of the steel pipe, and microcracks appear in the concrete inside, which leads to a significant increase in the longitudinal displacement of the specimen, and then the nominal stress-strain curve gradually deviates from the straight line. When the specimen enters the plastic stage, the nominal stress-strain curve of the specimen decreases. The descending section of the concrete-filled spiral external ribs steel pipe column (SSP-II) is particularly obvious, which is mainly due to the large plastic deformation on the surface of the steel pipe, resulting in the separation of the welding points between the external ribs and the steel pipe and the sharp reduction of the circumferential binding force. Compared with the SSP-II specimen, the descending section of the SSP-I specimen and concrete-filled ordinary steel pipe column is moderate.

Since the steel content of the concrete-filled gas drainage steel pipe short columns is lower than that of concrete-filled ordinary steel pipe columns, the restraint effect on the core concrete is slightly weaker, and the ultimate stress of specimen failure is also slightly smaller, but the contribution of steel per unit weight of gas drainage steel pipe to concrete reinforcement is higher than that of ordinary steel pipe.

3.3. Degradation of Axial Bearing Capacity and Secondary Strengthening. Defining the axial compression bearing capacity degradation coefficient of concrete-filled steel tubular specimens χ is the ratio of the valley β of the nominal stress-strain curve to the first peak stress λ, namely, $\chi = \beta/\lambda$. The rebound amplitude ψ of axial compression bearing capacity is defined as the ratio of the rebound peak stress ρ to the first peak stress λ, namely, $\psi = \rho/\lambda$, and the maximum stress after the rebound peak stress takes the first peak stress. χ and ψ of concrete-filled spiral welded steel pipe column (SSP-I), concrete-filled external rib spiral steel pipe column (SSP-II), and concrete-filled ordinary round steel pipe column (RSP) are shown in Table 3.

The average degradation range of axial compression bearing capacity of ordinary round steel is 81.90%, and the average recovery range of axial compression bearing capacity is 99.53%; the average degradation range of axial compression bearing capacity of SSP-I specimen is 70.38%, and the average recovery range is 96.75%; the average degradation range and recovery range of SSP-II specimen are only 34.47% and 60.58%, respectively. It is found that the post-peak load-bearing characteristics of SSP-I are better than those of SSP-II.

4. Discussion

4.1. Axial Load-Strain. Three types of specimen strain gauge sticking mode are completely consistent, as shown in Figure 6(a). Typical specimen is selected from each type of specimen for discussion. The axial strain at different positions of the specimen during loading can be measured by axial strain gauges pasted on the external surface of the specimen at different heights. The relationship between the axial load and the axial strain ε_a of the specimen is shown in Figure 5.

As shown in Figures 7(a) and 7(b), at the beginning of loading, the N-ε_a curve of SSP-I and SSP-II specimens increased linearly, and the axial strain at different heights was uniform. As the axial load continues to increase, the core concrete began to crack, and the external steel pipe began to play a constraint role. Due to the different damage degrees of concrete at different heights of the specimen, the steel pipe showed uneven deformation, and the N-$\boldsymbol{\varepsilon}_a$ relationship curve of the specimen at different heights showed "bifurcation." With the further increase in load, the strain of steel tube increases rapidly, and the N-ε_a curve shows a long plastic deformation platform until the axial strain gauge fails.

As can be seen from Figure 7(c), compared with SSP-I and SSP-II specimen, the concrete-filled ordinary round steel tube specimen shows uneven deformation at the initial stage of loading. With the increase in axial load, the difference increases gradually. When the load reaches 90% of the ultimate load, the strain gauge will be damaged due to the excessive axial deformation, but the data collected before failure have exceeded the yield strain of the steel tube, indicating that the cooperative working performance of concrete-ordinary steel pipes is weaker than that of concrete-gas drainage pipe.

4.2. Hoop Stress-Strain. The relationship curve between the stress and the hoop strain is shown in Figure 8.

It can be seen from Figures 8(a) and 8(b), at the beginning of loading, that the hoop strain of SSP-I and SSP-II specimens increases linearly with the increase in load but is smaller than the axial strain of the same period. At this time, the external steel pipe does not play a constraint role on concrete. As the axial load continues to increase, the external steel pipe begins to exert the restraint effect on the concrete, and the hoop stress-strain curves of SSP-I and SSP-II specimens at different heights also show "bifurcation," which is consistent with the characteristics of axial stress-strain curves, indicating that the deformation degree of the external surface of the specimens at different heights is quite different. As shown in Figure 8(c), the difference in the N-ε_h relationship curve of the concrete-filled ordinary round steel pipe specimens at different heights is small. The main reason is that the ordinary round steel pipe has split, as shown in

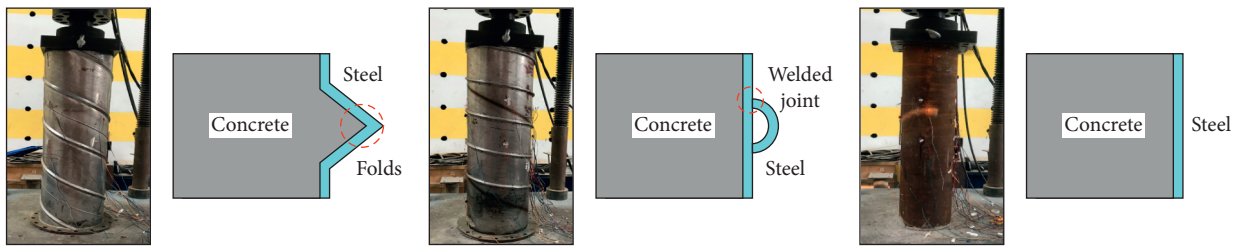

Figure 6: Characteristics of concrete-filled steel pipe interface with three cross section forms. Concrete raw materials are as follows: PO42.5 cement, natural river sand, 10 mm stone, HQ liquid alkali-free accelerator, Sulfate-based early strength agent, water. (a) SSP-I; (b) SSP-II; (c) RSP.

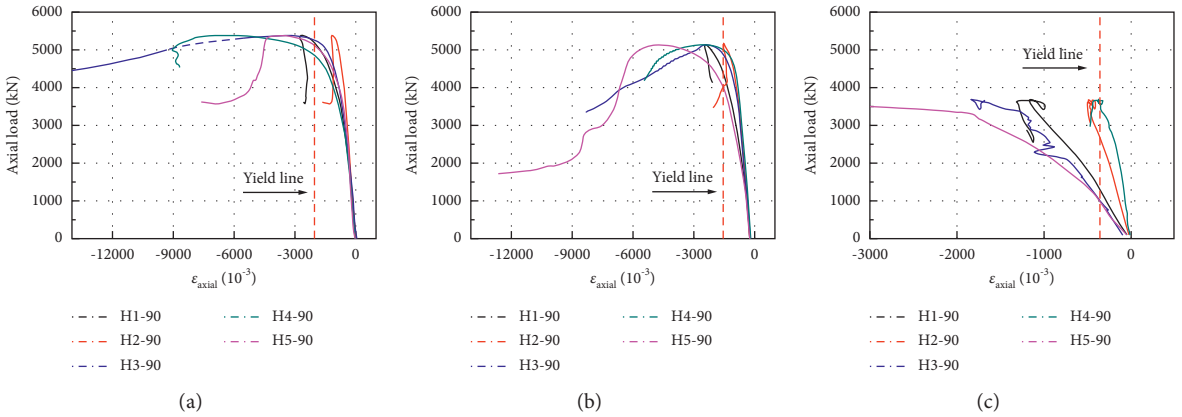

Figure 7: The axial load-strain curve of specimen. (a) SSP-I; (b) SSP-II; (c) RSP.

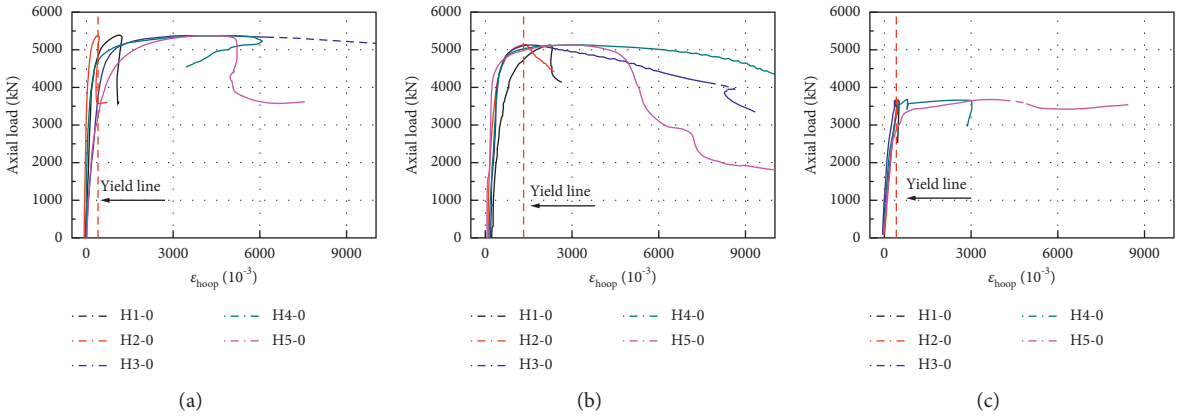

Figure 8: The hoop load-strain curve of specimen. (a) SSP-I; (b) SSP-II; (c) RSP.

Figure 5(c), and the collected stress-strain data cannot reflect the true hoop stress-strain relationship. In general, the cooperative performance of two kinds of gas drainage steel pipe with concrete is better than that of ordinary round steel pipe with concrete.

4.3. Numerical Simulation. ANSYS/LS-DYNA is mainly based on the Lagrange algorithm, with ALE algorithm and Euler algorithm. ANSYS preprocessing software is used to establish the numerical model and then modify the exported K file, and we used LSDYNA to analyze the problem. LS-PrePost post-processing software was used to view the output results [20].

The finite element method is used to simulate concrete-filled steel pipe columns under axial compression. The numerical model consists of three parts: concrete, steel pipe, and rigid body. Adopting a displacement constraint as the lower boundary condition on concrete-filled steel pipe columns specimens, we used the keyword

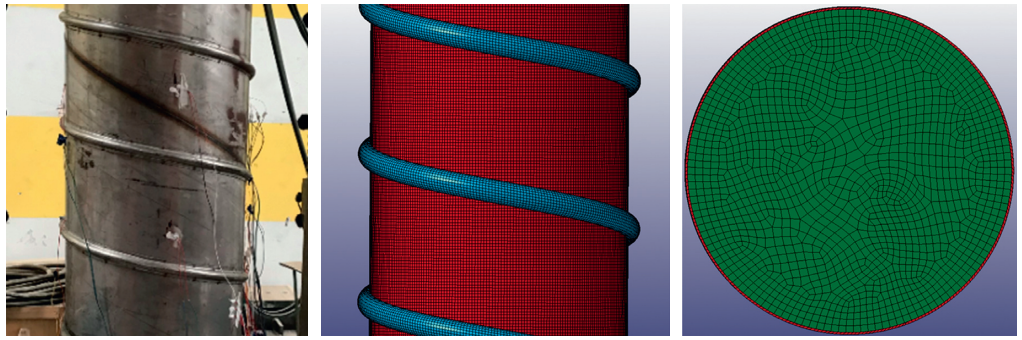

Figure 9: Establishment of the finite element model.

Table 4: Parameters used in the numerical model.

Concrete	Values	Rigid body/steel pipe	Values
Mass density	2400 kg/m^3	Mass density of rigid body	7850 kg/m^3
Unconfined compression strength	30 MPa	Young's modulus of rigid body	201 MPa
Young's modulus	27 MPa	Poisson's ratio of rigid body	0.3
Poisson's ratio	0.29	Mass density of steel pipe	7800 kg/m^3
Shear strain at failure	0.45	Young's modulus of steel pipe	206 GPa
Tensile strain at failure	−0.2	Poisson's ratio of steel pipe	0.29
Maximum aggregate size	19 mm	**	

*BOUNDARY_SPC_SET to bounding Y-direction displacements on all elements at the bottom of the simulated concrete-filled steel pipe columns to simulate the uniaxial compression testing of concrete-filled steel pipe columns by controlling the displacement of the simulated rigid body. Figure 9 is the establishment of the finite element model.

In the model, SOLID 164 solid elements were used to establish the numerical models. Concrete was simulated by using the *MAT_CSCM. Steel pipe was simulated by using the *MAT_ PLASTIC_KINEMATIC. And by modifying the parameters SIGP1 and EPSSH in the keyword *MAT_ADD_EROSION (erosion failure criterion), we could simulate the failure of specimens under uniaxial compression. For the rigid body, we used a *MAT_020 rigid model (*, *MAT_RIGID). Table 4 contains the parameters pertaining to the numerical modelling of the rigid body and concrete-filled steel pipe columns. The contact type of rigid body and concrete-filled steel pipe columns is modelled as a point-to-surface contact. The keyword is *CONTACT_NODES_TO_SURFACE.

The axial compressed characteristics of three kind of concrete-filled steel pipe short columns are simulated by the FE method. In the elastic-plastic stage, the simulated curves of SSP-I and SSP-II deviate from the measured curves. In the slowly descending section and the secondary strengthening section, the simulated values are slightly higher than the measured values, but the secondary strengthening characteristics of samples are well simulated. The simulation curve of ordinary circular steel tube specimen well reflects the stress-strain characteristics of the specimen in each stage, and the test results are in good agreement with the simulation results, as shown in Figure 10.

As shown in Figure 11, with the increase in axial load, the stress concentration zone appears on the weld position of SSP-I gas drainage steel pipe and the stress concentration zone extends along the spiral direction of the steel pipe. For the core concrete, the stress between the spiral weld is significantly higher than that between the weld position. The stress distribution near the convex weld of SSP-I specimen is complex. The convex weld forms a spiral pressure relief ring on the surface of the concrete column, and the pipe body between the spiral weld is the main constraint on the concrete. For SSP-II specimen, the stress concentration zone appears in root of spiral external rib and also extends along the spiral line. Since the loading end is on the top of the specimen, the concrete stress concentration area is located in the middle of the spiral outer ribs in the upper part of the specimen, which is mutually confirmed by the failure mode of the specimen. For ordinary round steel pipe specimens, the internal concrete showed irregular splitting failure, the steel pipe body at the loading end has a vertical tearing phenomenon, the steel pipe and the concrete have peeled off, and the longitudinal strain distribution of the specimen at different heights is quite different. This law is consistent with the strain curve in Figure 7. In general, because the diameter-thickness ratio of SSP-I and SSP-II is large, the overall restraint capacity of gas drainage pipe to concrete is slightly weaker than that of ordinary circular steel pipe, but the cooperative bearing capacity of SSP-I and SSP-II gas drainage pipes with concrete is better than that of ordinary steel pipes. In addition, the sharp decrease in stress of SSP-II specimen is mainly due to the sudden release of stress concentrated in the position of the external rib after the rib and the tube are broken away.

4.4. Theoretical Calculation of Ultimate Bearing Capacity. Many studies have been conducted on the ultimate bearing capacity of concrete-filled steel tube members. Among them,

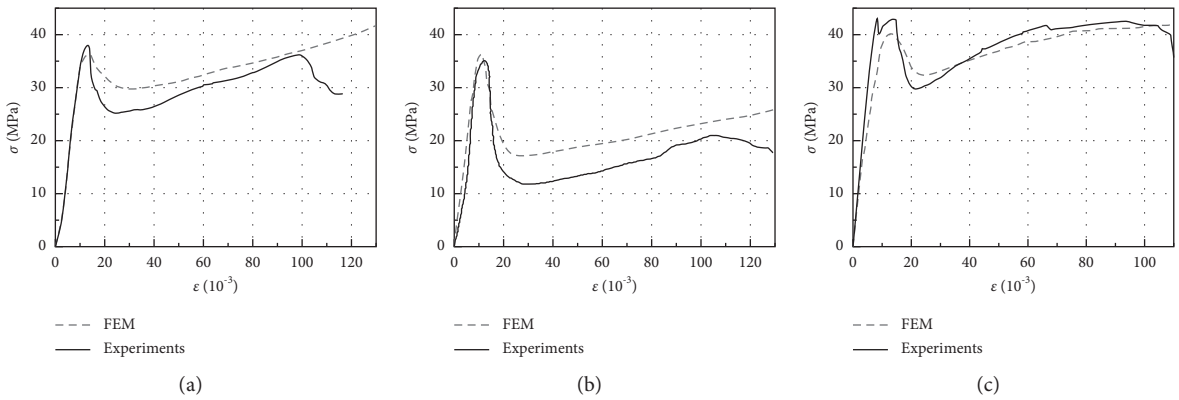

Figure 10: Comparison of simulation results and test curves: (a) SSP-I; (b) SSP-II; (c) RSP.

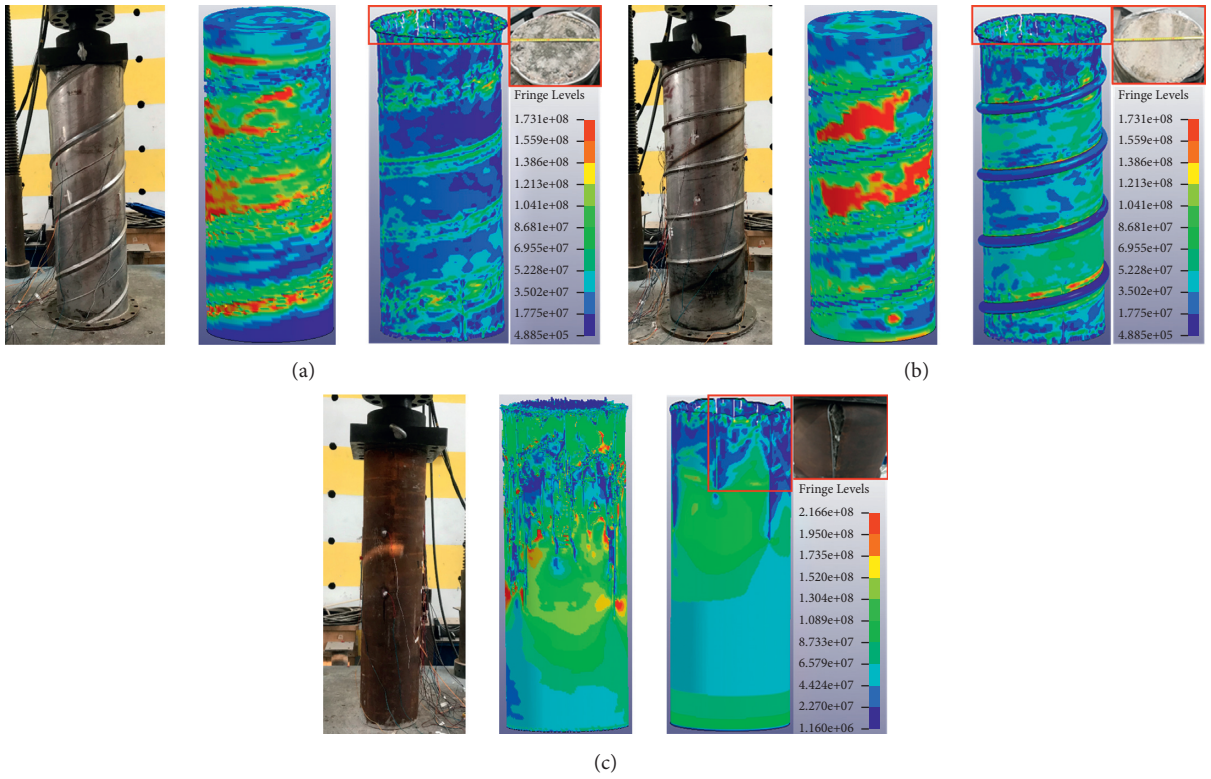

Figure 11: Simulation effect: (a) SSP-I; (b) SSP-II; (c) RSP.

the theories proposed for the ultimate bearing capacity of short columns under axial compression are mainly unified strength theory, limit equilibrium theory, and superposition theory. The unified strength theory involves Zhong Shantong equation (Zhong 2003) and Han Linhai equation (Han 2016), limit equilibrium theory involves CECS 28:2012 (2012), and superposition theory includes CECS 159:2004 (2004), Japanese standard aij-1997 (1997), European Association standard EC$-2004 (2004), and American Standard ACI-2005 (2005). In order to study whether the existing calculation method is suitable for SSP-I and SSP-II gas drainage steel pipe concrete-filled columns, the above formula is used to calculate the ultimate bearing capacity of the specimen under axial compression, the value N_c is calculated, and it is compared with the measured value N_u, as shown in Table 5.

For SSP-I and SSP-II samples, the calculated value based on Zhong Shantong's equation, Han Linhai's equation, and AIJ-1997 standard is slightly larger than the actual measured value. In addition, the calculated value of CECS 28:2012 based on the limit equilibrium theory is about 50% higher than the measured value. Therefore, according to the above theory, the ultimate bearing capacity design of SSP concrete columns under axial compression is risky. In contrast, the calculated value based on EC4-2004 and ACI-2005 standards is slightly lower than the actual measured value, the

Table 5: Comparison of measured and calculated results.

No.	N_u (kN)	Average value	Unified strength theory				Limit equilibrium theory		Superposition theory					
			Zhong Shantong equation		Han Linhai equation		CECS 28:2012		AIJ-1997		EC4-2004		ACI-2005	
			N_c (kN)	N_c/N_u	N_c (kN)	N_c/N_u	N_c (kN)	N_c/N_u	Nc (kN)	N_c/N_u	N_c (kN)	N_c/N_u	N_c (kN)	N_c/N_u
SSP-I-1	5386													
SSP-I-2	4836	5130	5436	1.059	5376	1.048	7635	1.488	5233	1.020	4864	0.948	4628	0.902
SSP-I-3	5170													
SSP-II-1	5132													
SSP-II-2	5385	5165	5436	1.052	5326	1.031	7635	1.478	5233	1.013	4864	0.941	4628	0.896
SSP-II-3	4979													
RSP-1	3678													
RSP-2	3651	3596	3798	1.056	3697	1.028	5036	1.400	3690	1.026	2893	0.804	2681	0.745
RSP-3	3459													

calculated value of ultimate bearing capacity under these standards is relatively conservative, and EC4-2004 is closer to the measured value. In order to take into account both safety and economy, the EC4-2004 standard is recommended to calculate the ultimate bearing capacity of concrete-filled SSP-I and SSP-II steel pipe columns.

5. Conclusion

In this paper, the axial compression performance test and numerical simulation analysis of two different types of concrete-filled gas drainage pipe columns and one type of concrete-filled ordinary round steel column specimen are carried out. The main conclusions are as follows:

(1) SSP-I and RSP specimens show good post-peak load-carrying properties. The secondary peak load of SSP-I and RSP specimens reached 70.38% and 81.92% of the ultimate load, respectively. In the process of secondary strengthening, the axial bearing capacity reaches 96.75% and 99.53% of the ultimate bearing capacity, respectively. When the SSP-II specimen reaches the ultimate load, causing a large strength attenuation, which attenuates to 34.47% of the ultimate load, the secondary strengthening load value is only 60.58% of the ultimate load.

(2) Two kinds of gas drainage steel pipes (SSP-I and SSP-II) show good cooperative performance with concrete in the process of axial compression test, and it gives full play to the binding effect on concrete. With the increase in load, the axial strain and hoop strain at different heights of the column are slightly different, and the core concrete is compressed into powder state. The hoop strain of ordinary concrete-filled steel tubular columns at different heights is uniform, but the axial strain is quite different.

(3) Secondary strengthening characteristics of SSP-I specimens are better than those of SSP-II specimens, and the numerical simulation results also shown that. Therefore, the SSP-I specimens are more suitable as the support component for gob-side entry retaining.

(4) The calculated values of Zhong Shantong equation, Han Linhai equation, AIJ-1997, and CECS 28:2012 are higher than the measured values. The calculated values of bearing capacity based on superposition theory EC4-2004 and ACI-2005 are relatively conservative, and the EC4-2004 standard is the closest to the measured value, so it is suggested to use EC4-2004 to calculate the ultimate bearing capacity of concrete-filled gas drainage steel tubular short column.

Data Availability

The data used to support the finding of this study are included within the article.

Conflicts of Interest

The authors declare that there are no conflicts of interest.

Authors' Contributions

Zi-Lu Liu and Zhan-Guo Ma conceived and established the experimental system. Ye Li carried out numerical simulation. Peng Gong guided thesis writing. Ke-Long Li and Wang Liu analyzed the data; Zi-Lu Liu wrote the paper.

Acknowledgments

This research was funded by the National Key Research and Development Projects of China, under Grant nos. 2019YEE0118500 and 2019YFC1904304; National Natural Science Foundation of China, under Grant nos. 52104107 and 51734009; Natural Science Foundation of Jiangsu Province, under Grant no. BK20200634; Fundamental Research Funds for the Central Universities, under Grant nos. 2021GJZPY05 and 2020ZDPY0218.

References

[1] M. C. He, G. Zhu, and Z. Guo, "Longwall mining "cutting cantilever beam theory" and 110 mining method in China - the third mining science innovation," *Journal of Rock Mechanics and Geotechnical Engineering*, vol. 7, no. 5, pp. 483–492, 2015.

[2] H. Luan, Y. Jiang, H. Lin, and G. Li, "Development of a new gob-side entry-retaining approach and its application," *Sustainability*, vol. 10, no. 2, p. 470, 2018.

[3] Q. Wang, M. He, J. Yang, H. Gao, B. Jiang, and H. Yu, "Study of a no-pillar mining technique with automatically formed gob-side entry retaining for longwall mining in coal mines," *International Journal of Rock Mechanics and Mining Sciences*, vol. 110, pp. 1–8, 2018.

[4] H. Yang, S. Cao, S. Wang, Y. Fan, S. Wang, and X. Chen, "Adaptation assessment of gob-side entry retaining based on geological factors," *Engineering Geology*, vol. 209, pp. 143–151, 2016.

[5] W.-d. Wu, J.-b. Bai, X.-y. Wang, Z.-j. Zhu, and S. Yan, "Field investigation of fractures evolution in overlying strata caused by extraction of the jurassic and carboniferous coal seams and its application: case study," *International Journal of Coal Geology*, vol. 208, pp. 12–23, 2019.

[6] Y. Chen, J. B. Bai, T. L. Zhu, S. Yan, S. H. Zhao, and X. C. Li, "Mechanisms of roadside support in gob-side entry retaining and its application," *Rock and Soil Mechanics*, vol. 33, pp. 1427–1432, 2012.

[7] P. Gong, Z. Ma, X. Ni, and R. Zhang, "Floor heave mechanism of gob-side entry retaining with fully-mechanized backfilling mining," *Energies*, vol. 10, no. 12, p. 2085, 2017.

[8] Z. G. Ma, P. Gong, and J. Q. Fan, "Coupling mechanism of roof and supporting wall in gob-side entry retaining in fully-mechanized mining with gangue backfilling," *International Journal of Mining Science and Technology*, vol. 21, no. 6, pp. 829–833, 2011.

[9] Y. Fang, C. Liu, H. Yang, and L. Yang, "Axial behavior of concrete-filled corrugated steel tubular column embedded with structural steel," *Journal of Constructional Steel Research*, vol. 170, Article ID 106064, 2020.

[10] M. Mohammadnejad, M. Naghipour, M. Nematzadeh et al., "Experimental and analytical investigation of the effect of external pressure on compressive behavior of concrete-filled steel pipe stub columns," *Applied Ocean Research*, vol. 100, Article ID 102152, 2020.

[11] Z. Wang, X. Zhou, F. Wei, and M. Li, "Performance of special-shaped concrete-filled square steel tube column under axial compression," *Advances in Civil Engineering*, vol. 2020, Article ID 1763142, 16 pages, 2020.

[12] J. Ci, H. Jia, S. Chen, W. Yan, T. Song, and K.-S. Kim, "Performance analysis and bearing capacity calculation on circular concrete-filled double steel tubular stub columns under axial compression," *Structure*, vol. 25, pp. 554–565, 2020.

[13] M. Ahmed, Q. Q. Liang, V. I. Patel, and M. Hadi, "Behavior of circular concrete-filled double steel tubular slender beam-columns including preload effects," *Engineering Structures*, vol. 220, Article ID 111010, 2020.

[14] Y.-B. Wang and J. Y. R. Liew, "Constitutive model for confined ultra-high strength concrete in steel tube," *Construction and Building Materials*, vol. 126, pp. 812–822, 2016.

[15] Y. Huang, Y. Sun, H. Sun, and Q. Wang, "Theoretical analysis on mechanical behavior of axially loaded recycled aggregate concrete filled steel tubes," *Mathematical Problems in Engineering*, vol. 2015, Article ID 270469, 14 pages, 2015.

[16] M. Ahmed, Q. Q. Liang, V. I. Patel, and M. N. S. Hadi, "Numerical analysis of axially loaded circular high strength concrete-filled double steel tubular short columns," *Thin-Walled Structures*, vol. 138, pp. 105–116, 2019.

[17] W. P. Huang, Q. Yuan, Y. L. Tan et al., "An innovative support technology employing a concrete-filled steel tubular structure for a 1000-m-deep roadway in a high in situ stress field," *Tunnelling and Underground Space Technology*, vol. 73, pp. 26–36, 2018.

[18] W. Huang, X. Wang, Y. Shen, F. Feng, K. Wu, and C. Li, "Application of concrete-filled steel tubular columns in gob-side entry retaining under thick and hard roof stratum: a case study," *Energy Science & Engineering*, vol. 7, no. 6, pp. 2540–2553, 2019.

[19] P. Wang, L. Ding, Y. Ma et al., "A case study on gob-side entry retaining technology in the deep coal mine of Xinjulong, China," *Advances in Civil Engineering*, vol. 2020, Article ID 8849093, 2020.

[20] Y. Li, S. Q. Yang, and Y. Li, "Experiment and numerical simulation on cracking behavior of marble containing double elliptic holes under uniaxial compression," *Theoretical and Applied Fracture Mechanics*, vol. 112, Article ID 102928, 2021.